Generalized Stability Theory. Part I: Autonomous Operators

BRIAN F. FARRELL AND PETROS J. IOANNOU*

Department of Earth and Planetary Sciences, Harvard University, Cambridge, Massachusetts

(Manuscript received 19 July 1995, in final form 31 January 1996)

ABSTRACT

Classical stability theory is extended to include transient growth processes. The central role of the nonnormality of the linearized dynamical system in the stability problem is emphasized, and a generalized stability theory is constructed that is applicable to the transient as well as the asymptotic stability of time-independent flows. Simple dynamical systems are used as examples including an illustrative nonnormal two-dimensional operator, the Eady model of baroclinic instability, and a model of convective instability in baroclinic flow.

1. Introduction

A central goal of high Reynolds number fluid dynamics in general and of theoretical meteorology in particular is to gain a comprehensive understanding of the origin and growth of perturbations in background flows characterized by available energy either baroclinic or barotropic. In barotropic flows the straining field of velocity provides the source of energy, while in baroclinic flows it is the potential energy of the geostrophically balanced jet that is tapped by growing perturbations. In all cases including mixed baroclinic–barotropic flows, the availability of energy for perturbation growth can be determined by linearizing the equations of motion about the appropriate background flow and searching for growing perturbations. If all possible perturbations are examined and only decaying ones are found, then it is certain that the background flow will persist when subjected to a sufficiently small disturbance. However, determining the potential for growth of all possible perturbations has not been the historical course of inquiry in stability theory. Rather, traditional stability theory, as exemplified by the baroclinic instability theories of Eady (1949) and Charney (1947), adopted the program of Rayleigh (1880) according to which instability is traced to the existence of exponentially growing modes of the linearized dynamic equations. The classical application of the normal-mode paradigm envisions unstable modes growing exponentially from infinitesimal beginnings over a large number of e-foldings so that the exponential mode of greatest growth eventually emerges as a finite-amplitude wave. This assumption of undisturbed growth is necessary to ensure the asymptotic dominance of the most rapidly growing normal mode, which in turn permits the theory to make predictions concerning the structure of observed waves of finite amplitude. In addition to applications of modal theory to the origin and structure of developing cyclones, attempts were made to extend normal-mode theory into the nonlinear regime by life cycle modeling (Simmons and Hoskins 1978) and to construct parameterizations of nonlinear equilibration processes founded on modal instability theory (Green 1970; Held 1978; Stone 1978).

Despite the wide acceptance accorded the normal mode theory of instability in all branches of high Reynolds number fluid dynamics, there remained difficulties of correspondence between the observed temporal variation and spatial structure of growing perturbations and the time independent structure of the normal modes (Petterssen 1955; Eliassen 1956). Such discrepancies and lingering theoretical questions involving the need to complete the normal modes in the case of linear inviscid dynamics by inclusion of a continuous spectrum of singular neutral modes led to reexamination of the results of Kelvin (1887) and Orr (1907) on the stability of the continuous spectrum by Case (1960) and Pedlosky (1964). These inquires showed that the continuous spectrum is stable in the sense that it fails to produce unbounded growth in the limit $t \to \infty$ and this negative result was generally interpreted as a proof assuring that the stability of a flow could be determined solely from inspection of its modal spectrum for exponential instabilities. However, it is now more widely appreciated that the modal spectrum only determines

* Additional affiliation: Division of Astrophysics, Astronomy and Mechanics, Department of Physics, University of Athens, Athens, Greece.

Corresponding author address: Dr. Brian F. Farrell, Department of Earth and Planetary Sciences, Harvard University, Pierce Hall, 29 Oxford Street, Cambridge, MA 02138.
E-mail: farrell@io.harvard.edu

stability in the $t \to \infty$ limit and that a more general analysis is necessary to determine the stability properties at finite time. Given that all experiments are conducted in finite time and that the timescale for cyclogenesis is typically 12–48 hours (Roebber 1984), finite-time stability analysis would seem to be the more appropriate, and indeed inquiry shows that in the quasigeostrophic system there are nonmodal transient disturbances at synoptic scale with large growth rates on timescales of a day or two (Farrell 1982a, 1984, 1985, 1989a; Montgomery and Farrell 1992). In addition, transient disturbances that develop on the planetary scale have been identified (Farrell 1988a; Borges and Hartman 1992; Chang and Mak 1995; Buizza and Palmer 1995). The most rapidly growing of these disturbances exhibit transient structural evolution during development that characterizes observed midlatitude cyclogenesis and planetary scale disturbance growth.

Recognition that a large subset of perturbations distinct from exponential modes grow by exploiting both the barotropic and baroclinic energy of the mean flow, including the energy associated with downstream variation of jets in diffluence and confluence (Farrell 1989b), allows the great variety of observed transient development processes to be subsumed under a single generalized stability theory. Freed of concentrating on the $t \to \infty$ asymptotic, this generalized stability theory allows a much closer correspondence to be made with observed structures that are highly variable both temporally and structurally.

Another problem of central importance to meteorology but traditionally distinct from the problems of synoptic-scale cyclogenesis and planetary-scale disturbance amplification is that of forecast accuracy and the predictability of atmospheric flows. The study of predictability is naturally posed as an initial value problem with the small error in the observations serving as the perturbation. Understanding of error growth based on modal instability was recently challenged by the observation that the observed predictability of flow regimes is unrelated to the modal instability of the flow (Palmer 1988). This and related evidence subsequently led to a reexamination of the basis of predictability theory in modal instability theory and increasing recognition that nonmodal processes dominate error growth in the linear regime (Lorenz 1965; Lacarra and Talagrand 1988; Farrell 1990; Moore and Farrell 1992; Molteni and Palmer 1993; Mureau et al. 1993; Vukicevic 1993; Ehrendorfer and Errico 1995).

In addition, the existence of a subspace of growing disturbances also suggests a mechanism by which the aggregated growth of individual structures supports the statistically steady variance of the fully turbulent flow. It can be shown that the net source of energy to the perturbation field attributable to nonlinear interactions among waves vanishes, and it follows that extraction of energy from the forced background flow by the subspace of growing disturbances, which is fully described by linear dynamics, must be responsible for maintaining eddy energy in the fully developed turbulent state (Joseph 1976; Henningson and Reddy 1994). This observation suggests a mechanistic model for the turbulent state in which the mean flow is subjected to continuous perturbative forcing (Farrell and Ioannou 1993c, 1994a, 1995; DelSole and Farrell 1995). The appropriate method of analysis for such a turbulence model is the stochastic dynamics of nonnormal linear systems.

While generalized stability theory was being developed in a meteorological context (Farrell 1988a, 1989a; Farrell and Ioannou 1993b, 1993f, 1994b, 1995; Ioannou 1995), a parallel development occurred in the study of transition to turbulence in laboratory shear flows where the nonnormality of the operator has been associated with the mechanism of by-pass transition (Farrell 1988b; Boberg and Brosa 1988; Gustavsson 1991; Butler and Farrell 1992; Reddy et al. 1993; Trefethen et al. 1993; Reddy and Henningson 1993; Farrell and Ioannou 1993c, 1993d, 1993e, 1994a; Breuer and Kuraishi 1994; Gebhardt and Grossmann 1994; Baggett et al. 1995). Because of the fundamental role of stability theory in dynamics we expect that generalized stability theory will be widely applicable, and indeed some novel applications have recently been identified including instability of stratified flows (Farrell and Ioannou 1993f), instability of ocean currents (Farrell and Moore 1992; Moore and Farrell 1993), coupled ocean–atmosphere system stability (Blumenthal 1991; Penland and Sardeshmukh 1995; Moore and Kleeman 1996, manuscript submitted to *Quart. J. Roy. Meteor. Soc.;* Kleeman and Moore 1996, manuscript submitted to *J. Atmos. Sci.*), granular flow (Schmid and Kytomaa 1994), magnetohydrodynamics (Farrell and Ioannou 1996, manuscript submitted to *Geophys. Astrophys. Fluid Dyn.*), and control of shear turbulence in laboratory flows (Farrell and Ioannou 1996).

The elements of generalized stability theory are examined below using simple dynamical systems as model problems. We begin in part I with asymptotic and finite-time stability analysis and progress to the stochastic dynamics of fully turbulent flow.

2. Response of nonnormal dynamical systems to impulsive excitation

The equation governing first-order perturbation dynamics in the atmosphere is a special case of the general linear dynamical system:

$$\frac{d\mathbf{u}}{dt} = \mathbf{A}\mathbf{u}, \tag{1}$$

in which $\mathbf{u}(t)$ is the state function representing the system at time t and $\mathbf{A}$ is the linearized dynamical operator.

In all problems involving the Navier–Stokes equations in bounded domains the spectrum of the operator $\mathbf{A}$ is discrete (Drazin and Reid 1981). Nonnormal growth pro-

cesses can be analyzed in terms of interaction among two or more of these discrete nonorthogonal modes. The exact number of modes involved in a particular instance of nonmodal growth will vary with the example and is not of fundamental significance. Fundamental significance attaches rather to the distinction between the modal growth of a single exponentially unstable eigenmode and nonmodal growth resulting from the interaction of two or more nonorthogonal eigenmodes.[1]

In the following it is assumed that (1) has been discretized so that $\mathbf{u}(t)$ is a state vector and $\mathbf{A}$ is the associated linearized dynamical matrix operator.[2] If the background state is steady so that $\mathbf{A}$ is not a function of time, then the dynamical system (1) is autonomous and the solution is explicit:

$$\mathbf{u}(t) = e^{\mathbf{A}t}\mathbf{u}(0). \tag{2}$$

In any case, there is a propagator matrix $\Phi_{[t,0]}$ that advances the system in time:

$$\mathbf{u}(t) = \Phi_{[t,0]}\mathbf{u}(0). \tag{3}$$

Only the existence of a propagator is required for the following development, and stationarity is assumed for convenience only.

The central distinguishing attribute of $\mathbf{A}$ that determines its transient dynamics is its normality, that is, whether or not $\mathbf{A}\mathbf{A}^\dagger = \mathbf{A}^\dagger\mathbf{A}$. If $\mathbf{A}$ commutes with its Hermitian transpose, here indicated by the superscript dagger, then $\mathbf{A}$ is normal and has a complete set of orthogonal eigenvectors. Perturbation growth rate for a normal $\mathbf{A}$ is bounded above by the member of the eigenspectrum of $\mathbf{A}$ [denoted by $\Lambda(\mathbf{A})$] with maximum real part. This maximum growth rate for normal operator is indicated by $\lambda^R_{\max}(\mathbf{A}) \equiv \max\{\mathrm{Re}[\Lambda(\mathbf{A})]\}$ and is referred to as the spectral abscissa of $\mathbf{A}$. In the case of a normal $\mathbf{A}$, the spectral norm of the propagator is given by $\|e^{\mathbf{A}t}\| = e^{\lambda^R_{\max}(\mathbf{A})t}$, where $\|\cdot\|$ indicates the spectral norm of a matrix that is defined to be the maximum singular value of the matrix. The stability of a normal dynamical system is determined for all time by its eigenspectrum. One example of a normal dynamical system in hydrodynamics arises in the analysis of the onset of convection in motionless background flows (the Rayleigh–Benard problem). In contrast to the lack of correspondence between observations and predictions based on normal-mode instability mentioned above in connection with nonnormal shear flow stability problems, observations have extensively verified exponential instability theory in normal dynamical systems such as the Rayleigh–Benard onset of convection problem (Drazin and Reid 1981; Henningson and Reddy 1994).

Because the finite-time perturbation dynamics of a nonnormal operator cannot be ascertained from the spectrum of the operator, it is necessary to generalize ideas of perturbation growth by considering the growth, σ, of an arbitrary perturbation $\mathbf{u}(0)$ over time t:

$$\begin{aligned}\sigma^2 &= \frac{(\mathbf{u}(t), \mathbf{u}(t))}{(\mathbf{u}(0), \mathbf{u}(0))} \\ &= \frac{(e^{\mathbf{A}t}\mathbf{u}(0), e^{\mathbf{A}t}\mathbf{u}(0))}{(\mathbf{u}(0), \mathbf{u}(0))} \\ &= \frac{(e^{\mathbf{A}^\dagger t}\, e^{\mathbf{A}t}\mathbf{u}(0), \mathbf{u}(0))}{(\mathbf{u}(0), \mathbf{u}(0))}.\end{aligned} \tag{4}$$

In the last equation of (4), the definition of the adjoint (Courant and Hilbert 1962) for the inner product $(\cdot, \cdot)$ that generates the Euclidean norm for the vector space: $\|\cdot\| = (\cdot, \cdot)^{1/2}$ has been used. It follows from (4) that a complete set of orthogonal perturbations $\mathbf{u}(0)$ can be ordered in growth over time t by eigenanalysis of the matrix: $e^{\mathbf{A}^\dagger t}\, e^{\mathbf{A}t}$. In particular, the greatest growth over time t as measured by the square of the Euclidean norm is given by the maximum eigenvalue of $e^{\mathbf{A}^\dagger t}\, e^{\mathbf{A}t}$ indicated by $\lambda_{\max}(e^{\mathbf{A}^\dagger t}\, e^{\mathbf{A}t})$, which is also equal to $\|e^{\mathbf{A}t}\|^2$ as can be also seen immediately from the singular-value decomposition of $e^{\mathbf{A}t}$ given in (5) below.

In the Euclidean norm the adjoint is the Hermitian transpose, but applications often require use of a norm other than the Euclidean. If the inner product is defined through the positive definite Hermitian form $\mathbf{M}$, that is, $(\mathbf{u}, \mathbf{u}) \equiv \mathbf{u}^\dagger\mathbf{M}\mathbf{u}$ then the associated vector norm is $\|\mathbf{u}\| \equiv (\mathbf{u}^\dagger\mathbf{M}\mathbf{u})^{1/2}$. We can choose new variables $\mathbf{v} = \mathbf{M}^{1/2}\mathbf{u}$ so that the dynamical system in $\mathbf{v}$ is governed by the

[1] Some confusion has arisen in the literature in connection with the continuous spectrum of inviscid and zonally homogeneous model problems, especially in relation to the Couette and Eady problems. The real number continuum of singular neutral modes in these problems cannot be placed in correspondence with the discrete spectrum of modes in their counterpart viscous or zonally inhomogeneous problems no matter how small the viscosity or zonal inhomogeneity. It follows that the inviscid and homogeneous modeling assumptions are singular perturbations to the physical problem and correspondence between the physical problem and these model problems must be made with care. This issue of correspondence was addressed by Lin (1961) as it relates to the Euler equation. Discrete approximations to the nonnormal continuous spectrum of the Couette, Eady, and similar problems are found to produce through interaction among the nonorthogonal approximations to the singular spectrum components propagators convergent with those produced by interactions among the nonorthogonal approximations to the analytic discrete modes in the nonsingular counterparts to these problems in which viscosity and/or zonal inhomogeneity has been taken into account. As mentioned previously, no correspondence is possible between the approximations to the singular modes and the approximation to the analytic modes themselves. Familiarity and analytical simplicity are advantages of the Couette- and Eady-type problems, but if in doubt one can confirm results obtained with the continuum spectrum of singular neutral modes by appealing to the corresponding physically correct problem with discrete analytic modes.

[2] The approximation of continuous functions and operators by their discrete counterparts is universal in practice but poses some serious analytical questions. There is reason to believe that continuous dynamical systems are convergent with their discrete approximations on bounded domains in space and time (Ince 1926). Asymptotic validity in time is not assured and there exist nonphysical examples in which the temporal asymptote of a finite-dimensional system does not converge as a function of resolution to the same asymptote as does its continuous counterpart (Zabczyk 1975).

new dynamical operator $D = \mathbf{M}^{1/2}\mathbf{A}\mathbf{M}^{-1/2}$ and (1) becomes $d\mathbf{v}/dt = \mathbf{D}\mathbf{v}$ with $\|\mathbf{v}\| = (\mathbf{v}^\dagger\mathbf{v})^{1/2} = \|\mathbf{u}\|$. It follows that we can always assume that analysis proceeds in the Euclidean norm. The choice of a norm should be made on physical grounds; ordinarily the energy norm is chosen although for a particular purpose a norm involving, for example, geopotential height may be more appropriate, and it is always possible to find a (usually unphysical) norm that renders the operator normal (cf. appendix in Farrell and Ioannou 1993c).

A singular-value decomposition (SVD) of the propagator (Noble and Daniel 1988; Golub and Van Loan 1989) reveals its complete set of unitary initial (columns of $\mathbf{V}$) and final (columns of $\mathbf{U}$) states, as well as the growth σ_i (along the diagonal of Σ) realized by each initial state as it is transformed under the action of the propagator into its associated final state:

$$e^{\mathbf{A}t} = \mathbf{U}\Sigma\mathbf{V}^\dagger. \tag{5}$$

The singular value decomposition can be visualized as the simultaneous formation of a particular orthogonal basis in the domain and range space of a matrix such that each unit orthogonal basis vector in the domain space $\mathbf{V}_i$ is mapped to a corresponding orthogonal basis vector $\mathbf{U}_i$ in the range space. The magnitude of each range vector under the transformation is given by the corresponding element of the diagonal matrix Σ.

The particular vectors $\mathbf{V}_i$ are ordered by growth. The initial condition that gives the maximum growth at a given time is referred to as the optimal perturbation at that time, and, by extension, the ordered columns of $\mathbf{V}$, each $\mathbf{V}_i$ of which is optimal subject to the constraint of orthogonality with the preceding $i - 1$ vectors, are referred to as the optimal basis. The maximum growth that occurs when all time intervals are examined is called the global optimal.

It is easy to show that the maximum growth that can be attained over a given time, t, is greater or equal to that attained by the fastest growing mode during the same time and similarly the minimum growth attained is at most equal to that due to the least-growing mode, that is,

$$\sigma_{\min}^2 \leqslant e^{(\lambda_i + \lambda_i^*)t} \leqslant \sigma_{\max}^2, \tag{6}$$

where λ_i ranges over all the eigenvalues of $\mathbf{A}$.

The most effective excitation of a given eigenmode of an N dimensional operator $\mathbf{A}$ with simple eigenvalues can also be determined by application of the singular value decomposition. The most effective excitation of a given eigenvector is defined to be the unit vector with largest projection on that eigenvector. As we show below, the most effective excitation of the eigenvector associated with the spectral abscissa $\lambda_{\max}^R(\mathbf{A})$ is also the optimal excitation in the limit $t \to \infty$. In the case of a normal operator it follows from the orthogonality of the eigenvectors that this unit vector of maximal projection coincides with the mode itself. However, this is not the case for nonnormal operators, the eigenvectors of which are not orthogonal. In two dimensions it is easy to see geometrically that for nonorthogonal real basis vectors (corresponding to eigenvectors of a nonnormal operator) the unit vector giving maximal projection on one basis vector is the orthogonal to the other basis vector, that is, the vector of maximal projection is the biorthogonal of the eigenvector we want to excite (see Fig. 1). It can be seen from Fig. 1 that the projection is larger when the angle between the two basis vectors is smaller. This argument can be generalized to higher-dimensional spaces with complex eigenvectors by use of the projector operator on the mode we wish to optimally excite.

There are two asymptotic limits of interest in connection with the excitation of the propagator. In the limit $t \to \infty$, maximum growth is obtained by the eigenfunction associated with the eigenvalue with maximum real part, just as normal-mode theory would suggest. To see this, consider the matrix $\mathbf{E}$ constructed by arranging the eigenvectors of $\mathbf{A}$ as columns in order of growth rate together with the diagonal matrix, Δ, of the associated modal growth factors, from which the following similarity transformation of the propagator can be constructed:

$$e^{\mathbf{A}t} = \mathbf{E}e^{\Delta t}\mathbf{E}^{-1}. \tag{7}$$

In the limit $t \to \infty$, the first column of $\mathbf{E}$ and the first row of $\mathbf{E}^{-1}$ exponentially dominate with amplification factor $e^{\text{Real}(\Delta_{11})t}$:

$$\lim_{t\to\infty} e_{\alpha\beta}^{\mathbf{A}t} = \mathbf{E}_{\alpha 1}e^{\Delta_{11}t}\mathbf{E}_{1\beta}^{-1}. \tag{8}$$

It can be seen by appeal to Schwartz's inequality that the initial condition of unit norm producing maximum growth over time t is the complex conjugate of $\mathbf{E}_{1\beta}^{-1}$,

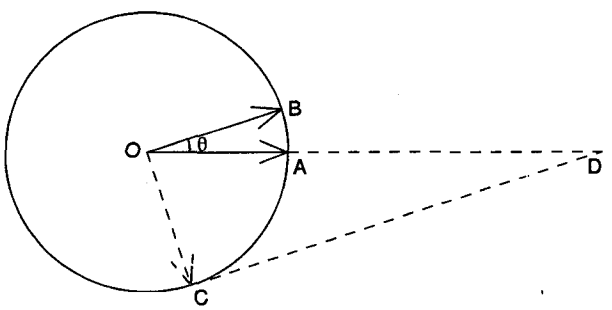

FIG. 1. Geometrical demonstration in two dimensions of the argument that the optimal excitation of a given eigenvector (OA) is its biorthogonal (OC) that can be identified with its associated adjoint eigenvector. Consider two eigenvectors OA, OB (solid arrows) subtending an angle θ. The unit vector OC (dotted arrow) maximally projecting on the eigenvector aligned with the x-axis (OA) is that perpendicular to the other eigenvector OB. This unit optimal (OC) is seen to produce on projection on OA the vector OD with magnitude $\csc(\theta)|\text{OA}|$.

which is the conjugate of the biorthogonal of the leading eigenvector rather than the leading eigenvector itself:

$$\lim_{t\to\infty} e^{\mathbf{A}t}_{\alpha\beta}(\mathbf{E}^{-1}_{1\beta})^* = \mathbf{E}_{\alpha 1}e^{\Delta_{11}t}. \tag{9}$$

Modal theory correctly predicts that in the limit $t \to \infty$, the eigenvector that has associated eigenvalue with maximum real part dominates. Not so obvious is the fact that the optimal initial condition with which to excite that mode is the conjugate of the biorthogonal of the dominant mode rather than the mode itself. In highly nonnormal systems such as the atmosphere, a mode and its biorthogonal differ greatly and the perturbation that optimally excites a mode bears little resemblance to the mode itself (Farrell 1988a, 1989a).[3]

Given the observed mean timescale for cyclogenesis of 24 hours (Roebber 1984), the $t \to \infty$ asymptotic is not likely to provide a realistic precursor for the cyclogenesis process on the forecast timescale. Of greater utility for this purpose is analysis of the $t \to 0$ limit of (4), which controls the initial growth of perturbations. Analysis of this limit provides the maximum possible instantaneous growth rate and the structure that produces this maximum growth rate, in addition to supplying other information such as the rate of expansion of the error ellipse in the short time forecast limit and those structures that contribute most to the short time error growth. The maximum instantaneous growth rate and the perturbation of maximum instantaneous growth itself also provides a constructive nonlinearly valid bound on the potential for perturbation growth in the flow (Joseph 1976).

The limit as $t \to 0$ is easily obtained by Taylor expansion of the matrix $e^{\mathbf{A}^\dagger t}e^{\mathbf{A}t}$ in (4):

$$\begin{aligned} e^{\mathbf{A}^\dagger t}e^{\mathbf{A}t} &\approx (\mathbf{I} + \mathbf{A}^\dagger t)(\mathbf{I} + \mathbf{A}t) \\ &= \mathbf{I} + (\mathbf{A} + \mathbf{A}^\dagger)t + \mathbf{O}(t^2), \end{aligned} \tag{10}$$

where $\mathbf{I}$ is the identity matrix. It follows that a tight upper bound on instantaneous growth rate, designated as $\alpha(\mathbf{A})$ and referred to as the numerical abscissa of $\mathbf{A}$, and the structure producing this maximum instantaneous growth rate can be found by eigenanalysis of the matrix $\mathbf{A} + \mathbf{A}^\dagger$. The maximum eigenvalue of $(\mathbf{A} + \mathbf{A}^\dagger)/2$ and its associated eigenvector provide the required growth rate and structure. Eigenanalysis of $\mathbf{A} + \mathbf{A}^\dagger$ typically reveals that high growth rates over short times can be realized in baroclinic flows even though all normal modes of $\mathbf{A}$ are damped.

[3] While the biorthogonal vector is the associated adjoint vector it may happen that boundary conditions on the adjoint of an operator do not coincide with boundary conditions imposed on the operator itself requiring slight modification of the adjoint vector (biorthogonal vector) in the vicinity of the boundary to meet the physical boundary conditions required by an initial perturbation. In any case optimal initial conditions obtained from S.V.D. of the propagator (5) necessarily satisfy physical boundary conditions.

The most relevant timescales for development in the atmosphere lie between the asymptotic limits $t \to 0$ and $t \to \infty$ and for these intermediate timescales the initial and final structures are found most easily from the SVD analysis of the propagator (5). Given that both asymptotic limits are subsumed, it is appropriate to refer to this analysis as the generalized stability analysis of the system (1).

3. Response of nonnormal dynamical systems to continuous excitation

a. Frequency domain analysis of continuously excited nonnormal forced systems

Asymptotically stable nonnormal dynamical systems exhibiting large transient response to impulsive forcing also exhibit enhanced asymptotic response to steady and harmonic forcing. An important problem in large-scale dynamics is determining the response of the atmosphere to steady forcing as is most commonly associated with the excitation of planetary waves by thermal and topographic inhomogeneities. Nonnormality of linearized planetary wave dynamics arises from the baroclinic–barotropic energy source associated with the midlatitude jet and this nonnormality produces greatly enhanced response to steady forcing, compared to the response of an equivalent normal system such as would be associated with solid-body rotation. The analysis presented in the previous section can be extended to the frequency domain to obtain the optimal response to harmonic forcing at any frequency including the special case of stationary forcing (Branstator 1985; Navarra 1993).

Consider the forced dynamical system

$$\frac{d\mathbf{u}}{dt} = \mathbf{A}\mathbf{u} + \mathbf{f}(t). \tag{11}$$

With the aid of the Fourier transform pair

$$\mathbf{u}(t) = \int_{-\infty}^{\infty} \hat{\mathbf{u}}(\omega)e^{i\omega t}d\omega, \tag{12}$$

$$\hat{\mathbf{u}}(\omega) = \frac{1}{2\pi}\int_{-\infty}^{\infty} \mathbf{u}(t)e^{-i\omega t}dt, \tag{13}$$

the response at frequency ω can be expressed as

$$\hat{\mathbf{u}}(\omega) = \mathbf{R}(\omega)\hat{\mathbf{f}}(\omega), \tag{14}$$

in terms of the resolvent

$$\mathbf{R}(\omega) = (i\omega\mathbf{I} - \mathbf{A})^{-1}, \tag{15}$$

where $\mathbf{I}$ is the identity.

In the case of normal systems, the largest response $\|\mathbf{R}(\omega)\|$ at a given frequency is obtained for a forcing with spatial structure corresponding to the eigenfunction with eigenvalue least removed from the forcing

frequency ω. The amplitude of this response is given by

$$\|\mathbf{R}(\omega)\| = \frac{1}{\text{dist}(i\omega, \Lambda(\mathbf{A}))}, \tag{16}$$

where dist denotes the shortest distance of ω from the spectrum of $\mathbf{A}$, $\Lambda(\mathbf{A})$. This is the familiar modal resonance in which the maximal response is obtained at the forcing frequency corresponding to the least stable eigenmode of the system and the square response is inversely proportional to the square of the damping rate.

For nonnormal systems, the previous conclusions have to be modified. In order to maximize

$$\|\hat{\mathbf{u}}(\omega)\|^2 = \hat{\mathbf{f}}(\omega)\mathbf{R}^\dagger(\omega)\mathbf{R}(\omega)\mathbf{f}(\omega), \tag{17}$$

we must select the optimal forcing to be the eigenvector associated with the maximum eigenvalue of $\mathbf{R}^\dagger(\omega)\mathbf{R}(\omega)$. Equivalently, SVD decomposition of the resolvent, $\mathbf{R} = \mathbf{U}\Sigma\mathbf{V}^\dagger$, allows identification of the optimal forcing with the column of $\mathbf{V}$ associated with the maximal singular value and identification of the resulting optimal response at ω with the corresponding column vector of $\mathbf{U}$. In particular, at $\omega = 0$ the $\mathbf{V}$ and $\mathbf{U}$ correspond respectively to the optimal forcing distribution and the EOF for forcing at zero frequency, as would be appropriate for the optimal excitation of waves by stationary distributions of thermal and topographic forcing. It is not the case, however, that the maximum response occurs at the frequency corresponding to the least-damped mode, as was the case for normal systems. Moreover, the response to harmonic forcing of systems exhibiting robust transient growth can be orders of magnitude greater than the response expected from traditional resonance arguments based on normal-system dynamics. This is of particular importance in the atmosphere where neglect of nonnormality results in a lack of correspondence between theory and observations of the frequency spectrum of the atmosphere, a discrepancy that is resolved by appropriate incorporation of the nonnormality of the midlatitude jet dynamics (Farrell and Ioannou 1994b, 1995).

To obtain an estimate for the optimal response, note that

$$(i\omega\mathbf{I} - \mathbf{A})^{-1} = \mathbf{E}(i\omega\mathbf{I} - \Delta)^{-1}\mathbf{E}^{-1}, \tag{18}$$

with Δ the diagonal eigenvalue matrix and $\mathbf{E}$ the matrix formed by the corresponding eigenvectors arranged in columns. The following bound can be obtained on the optimal response in terms of the spectral condition number $\kappa(\mathbf{E}) \equiv \|\mathbf{E}\|\,\|\mathbf{E}^{-1}\|$ and the distance of the forcing frequency ω to the spectrum of $\mathbf{A}$ (Kato 1976; Trefethen 1996, personal communication):

$$\|\mathbf{R}(\omega)\| \leq \frac{\kappa(\mathbf{E})}{\text{dist}(i\omega, \Lambda(\mathbf{A}))}, \tag{19}$$

indicating the possibility of greatly enhanced frequency response in nonnormal systems with nearly parallel eigenvectors resulting in eigenvector matrices with large spectral condition numbers, $\kappa(\mathbf{E})$. This result is most simply obtained in the context of pseudospectral analysis, which provides a systematic basis for analyzing the nonnormality of matrices and continuous operators (Trefethen 1991; Reddy et al. 1993; Reddy 1993; Trefethen et al. 1993).

When all frequencies are excited equally, as would be the case for componentwise uncorrelated white noise forcing of unit variance, that is, $\langle \hat{f}_i(\omega_1)\hat{f}_j^*(\omega_2)\rangle = \delta_{ij}\delta(\omega_1 - \omega_2)/2\pi$, the ensemble response variance is given by

$$\langle u^2 \rangle = \frac{1}{2\pi}\int_{-\infty}^{\infty} F(\omega)d\omega, \tag{20}$$

where

$$F(\omega) = \text{trace}(\mathbf{R}^\dagger(\omega)\mathbf{R}(\omega)), \tag{21}$$

and $\langle u^2 \rangle$ denotes the stationary ensemble variance.

The eigenvalues of the resolvent $\mathbf{R}$ are $(i\omega - \lambda_i)^{-1}$ in which λ_i are the eigenvalues of $\mathbf{A}$. It can be shown that

$$F(\omega) \geq \sum_{i=1}^{N} \frac{1}{|i\omega - \lambda_i|^2}, \tag{22}$$

with equality only when $\mathbf{A}$ is normal (Ioannou 1995). This inequality has the important implication that the variance as a function of frequency produced by spatially uncorrelated white noise forcing of a nonnormal dynamical system nearly always exceeds the variance obtained as a summation of the contributions from the poles of the resolvent, as is appropriate for the case of a normal operator. Interaction among the modes enhances the variance by drawing on the energy available from the background flow and an example of this phenomenon is the stochastic response of the midlatitude jet that greatly exceeds that anticipated solely from the damping of the system (Farrell and Ioannou 1994b; 1995).

It is important to appreciate the role of the eigenmodes in the maintenance of this large variance. In highly approximated model systems spanned solely by a continuum of singular modes, as is the case for constant shear flows in the Euler equation, only a modest increase of variance can be achieved by stochastic forcing of the system (Kraichnan 1976; Shepard 1985; Farrell and Ioannou 1993a). This is because nonnormal growth achieved in such systems by energetic interaction with the background flow is as quickly lost to the reverse process in the absence of a long-lived repository for perturbation energy in the form of discrete modes. The discrete spectrum of damped modes provides the requisite repository for the accumulation of nonnormal energy growth leading to the maintenance of enhanced levels of variance (Farrell and Ioannou 1993a, 1993b, 1994a; Ioannou 1995). The end result in marginally stable systems is a response close in fre-

quency to that of the least-damped mode, but with amplitude greatly exceeding that expected from normal resonance arguments.

b. Time domain analysis of nonnormal stochastic systems

Transient growth of disturbances in shear flow can be traced to a substantial subspace of perturbations that extract energy from the background flow. In section 2, analysis of these growing perturbations was framed as an initial value problem involving as a parameter the physically relevant interval in time over which growth occurs. Error growth in the predictability problem arises from the ensemble of growing perturbations that are excited by projection of the initial error on this growing subspace. By extension, growth of the subspace of perturbations that we have analyzed in connection with the cyclogenesis and predictability problems is also able to support a time-mean variance if the excitation mechanism operates continuously, as must be the case for a system with stationary statistics. The appropriate method of analysis for studying the maintenance of time-mean variance by continuous incoherent forcing is the stochastic dynamics of the associated nonnormal system.

The stochastically forced linear dynamical system can be written in the form

$$\frac{d\mathbf{u}}{dt} = \mathbf{A}\mathbf{u} + \mathbf{F}\boldsymbol{\eta}(t), \tag{23}$$

in which $\boldsymbol{\eta}(t)$ is a temporally Gaussian white-noise forcing componentwise δ correlated with zero ensemble mean and unit ensemble covariance:

$$\langle \boldsymbol{\eta}_i(t_1)\boldsymbol{\eta}_j^*(t_2)\rangle = \delta_{ij}\delta(t_1 - t_2). \tag{24}$$

The spatial distribution of the forcings is provided by the matrix $\mathbf{F}$, and if it is chosen to be unitary, the resulting statistics become independent of the particular choice of $\mathbf{F}$.

To obtain the stochastic growth of perturbations we first write the forced solution of (23) as

$$\mathbf{u}(t) = \int_0^t e^{\mathbf{A}(t-s)}\mathbf{F}\boldsymbol{\eta}(s)ds. \tag{25}$$

The variance maintained by this stochastic forcing is given in the Euclidean norm by

$$\begin{aligned}\langle \|\mathbf{u}(t)\|^2\rangle &= \left\langle \int_0^t ds \int_0^t ds' \boldsymbol{\eta}^\dagger(s)\mathbf{F}^\dagger e^{\mathbf{A}^\dagger(t-s)}e^{\mathbf{A}(t-s')}\mathbf{F}\boldsymbol{\eta}(s')\right\rangle \\ &= \mathbf{F}^\dagger\left(\int_0^t e^{\mathbf{A}^\dagger(t-s)}e^{\mathbf{A}(t-s)}ds\right)\mathbf{F} \\ &= \mathbf{F}^\dagger\mathbf{B}\mathbf{F},\end{aligned} \tag{26}$$

revealing that the hermitian operator

$$\mathbf{B}^t = \int_0^t e^{\mathbf{A}^\dagger s}e^{\mathbf{A}s}ds \tag{27}$$

accumulates the perturbation growth when all perturbations are stochastically excited. This operator should be compared with the operator $e^{\mathbf{A}^\dagger t}e^{\mathbf{A}t}$, eigenanalysis of which reveals the optimal perturbation growth as we have seen in the previous section. An alternative and computationally preferable method for calculating the stochastic dynamical operator $\mathbf{B}^t$ results from differentiating (27) with respect to time to obtain

$$\frac{d\mathbf{B}^t}{dt} = \mathbf{I} + \mathbf{A}^\dagger\mathbf{B}^t + \mathbf{B}^t\mathbf{A}, \tag{28}$$

in which $\mathbf{I}$ is the identity matrix.

In direct analogy with the analysis of optimal growth in the previous section, a complete set of orthogonal forcings forming the columns of a unitary $\mathbf{F}$ can be found for the stochastic variance at time t in (26) by eigenanalysis of the positive definite hermitian $\mathbf{B}^t$. If the operator $\mathbf{A}$ is asymptotically stable, a stationary solution is obtained in which the eigenfunctions of $\mathbf{B}^\infty$ are ordered according to their contribution to the variance of the statistically steady state. The forcings ordered in this way will be referred to as stochastic optimals.

The stochastic optimals most effectively excite the stationary variance and should be contrasted with the orthogonal structures that most effectively span the maintained variance, which are commonly referred to as the EOFs of the dynamical system. The stochastic optimals bear a relationship to the EOFs in the stochastic analysis analogous to that between the optimal excitation and the optimal response in the SVD analysis of the propagator of the initial value problem. To obtain the EOFs we need first to form the correlation matrix

$$\begin{aligned}\mathbf{C}_{ij}^t &= \langle \mathbf{u}_i(t)\mathbf{u}_j^*(t)\rangle \\ &= \left(\int_0^t e^{\mathbf{A}(t-s)}\mathbf{F}\mathbf{F}^\dagger e^{\mathbf{A}^\dagger(t-s)}ds\right)_{ij},\end{aligned} \tag{29}$$

which satisfies

$$\frac{d\mathbf{C}^t}{dt} = \mathbf{F}\mathbf{F}^\dagger + \mathbf{A}\mathbf{C}^t + \mathbf{C}^t\mathbf{A}^\dagger. \tag{30}$$

Each eigenvalue of the positive-definite hermitian operator $\mathbf{C}^t$ equals the variance accounted for, under unbiased forcing and at time t, by the pattern of its corresponding eigenvector, and the pattern that corresponds to the largest eigenvalue contributes most to the perturbation variance at t.

If $\mathbf{A}$ is normal and the forcing unitary ($\mathbf{F}\mathbf{F}^\dagger = \mathbf{I}$), then $\mathbf{A}$, $\mathbf{B}^t$, $\mathbf{C}^t$ commute and the stochastic optimals, the EOFs, and the modes of the dynamical system coincide. For such a system eigenanalysis of $\mathbf{A}$ suffices

for understanding the statistics of the perturbations in the linear limit. In contrast, for nonnormal systems the stochastic optimals, the EOFs and the modes of the dynamical operator are all distinct (Farrell and Ioannou 1993b, 1993c, 1995).

If $\mathbf{A}$ is asymptotically stable, the system approaches a statistically steady state as t increases, in which $\mathbf{B}^\infty$ and $\mathbf{C}^\infty$ satisfy the Lyapunov equations:

$$\mathbf{A}\mathbf{C}^\infty + \mathbf{C}^\infty\mathbf{A}^\dagger = -\mathbf{F}\mathbf{F}^\dagger$$
$$\mathbf{A}^\dagger\mathbf{B}^\infty + \mathbf{B}^\infty\mathbf{A} = -\mathbf{I}. \quad (31)$$

The Lyapunov equations in (31) are readily solved for $\mathbf{B}^\infty$ and $\mathbf{C}^\infty$ given the asymptotically stable operator $\mathbf{A}$ and the forcing correlation matrix $\mathbf{F}$.

4. Examples

a. A simple 2 × 2 system

Consider generalized stability analysis of the dynamical system governed by

$$\mathbf{A} = \begin{pmatrix} -1 & -\cot\theta \\ 0 & -2 \end{pmatrix}. \quad (32)$$

This matrix has associated matrix of column eigenvectors

$$\mathbf{E} = \begin{pmatrix} 1 & \cos\theta \\ 0 & \sin\theta \end{pmatrix}, \quad (33)$$

and has stable eigenvalues $(-1, -2)$ so that the following similarity transformation can be made:

$$\mathbf{A} = \mathbf{E}\begin{pmatrix} -1 & 0 \\ 0 & -2 \end{pmatrix}\mathbf{E}^{-1}. \quad (34)$$

The nonnormality of the operator is revealed by calculation of the commutator:

$$\mathbf{A}\mathbf{A}^\dagger - \mathbf{A}^\dagger\mathbf{A} = \cot\theta\begin{pmatrix} \cot\theta & 1 \\ 1 & -\cot\theta \end{pmatrix}, \quad (35)$$

which is seen to vanish only for $\theta = \pi/2$, in which case (32) is normal.

This is an asymptotically stable system with spectral abscissa $\lambda^R_{\max}(\mathbf{A}) = -1$ but with a potential for nonnormal growth that can be estimated from the numerical abscissa $\alpha(\mathbf{A})$, which as we have seen is the maximum instantaneous growth rate $\lim_{t\to 0}\|e^{\mathbf{A}t}\|$ given by the maximum eigenvalue of $(\mathbf{A} + \mathbf{A}^\dagger)/2$. This maximum instantaneous growth rate is easily seen to be

$$\alpha(\mathbf{A}) = \frac{-3 + \csc\theta}{2} \quad \text{for} \quad 0 < \theta < \pi/2, \quad (36)$$

which indicates the existence of an instantaneously growing perturbation for $\theta < \pi/9.244$. This unit norm perturbation of maximum instantaneous growth rate can be shown by eigenanalysis of $(\mathbf{A} + \mathbf{A}^\dagger)/2$ to be the unit vector subtending an angle $\theta_\alpha = \arctan(\sin\theta - 1/\cos\theta)$ with the x axis. As has been remarked, the choice $\theta = \pi/2$ renders the system normal, in which case it is immediate that the numerical abscissa coincides with the least decaying eigenvector that is oriented along the x axis with $\theta_\alpha = 0$. Nonnormality increases as $\theta \to 0$ with the vector of maximal instantaneous growth tending in this limit to the angle $\theta_\alpha = -\pi/4$. In addition there is also the direction of the maximally contracting vector that lies perpendicular to the direction of the maximally growing vector. These maximally growing and contracting directions are marked for $\theta = \pi/100$ in the phase plane diagram shown in Fig. 2. Subsequent evolution of a perturbation that starts in the direction of maximal instantaneous growth is shown in Fig. 3. Substantial excursion from the equilibrium position is seen to occur before ultimate asymptotic decay sets in. This transient excursion is analogous in an atmospheric context to a cyclogenesis event, resulting from the chance conjunction of upper- and lower-level potential vorticity anomalies. The dynamics of this transient phase would have been altogether missed if analysis had been limited to the decaying eigenspectrum of the operator.

To obtain the stability properties of the operator at times intermediate between the $t \to 0$ asymptotic controlled by the numerical abscissa and the $t \to \infty$ asymptotic controlled by the spectral abscissa, we must

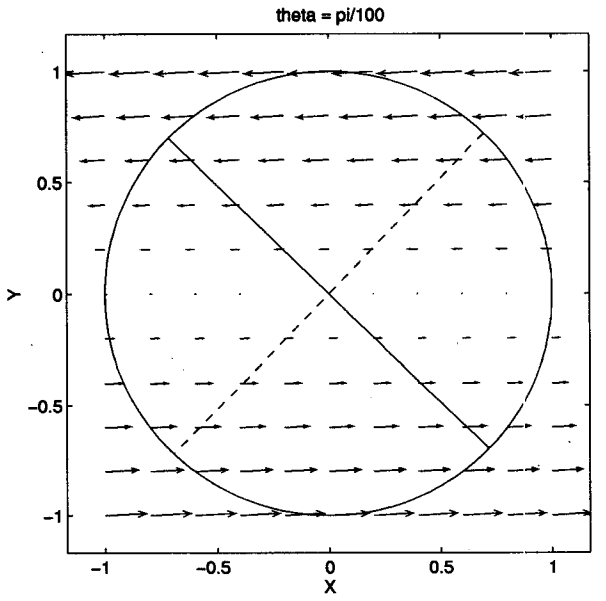

FIG. 2. Phase plane portrait of the vector field near the origin produced by the simple 2 × 2 non-normal matrix example with $\theta = \pi/100$. The unit eigenvector associated with the largest eigenvalue of $(\mathbf{A} + \mathbf{A})^\dagger/2$, the numerical abscissa, marked as a continuous line, and the least growing eigenvector of $(\mathbf{A} + \mathbf{A})^\dagger/2$ as the dashed line. The intersection of the former with the unit circle is the instantaneously most rapidly growing unit vector which will be integrated forward in the example.

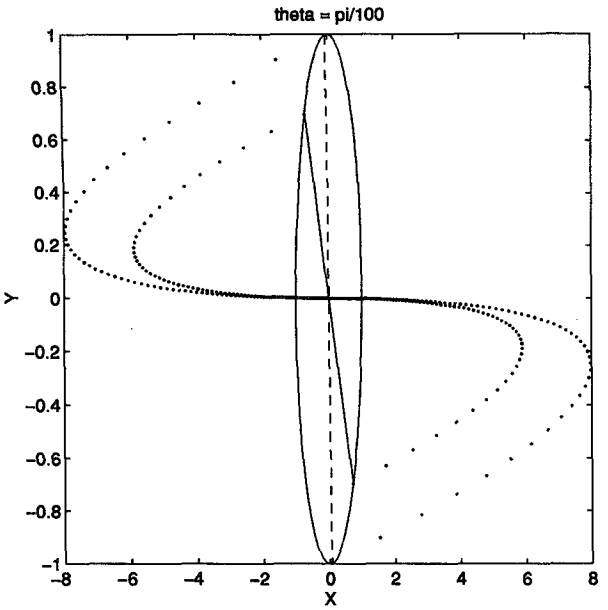

FIG. 3. Phase plane portrait of trajectories of the simple 2 × 2 nonnormal matrix example with $\theta = \pi/100$. Shown are the trajectory with initial condition of the eigenvector with the maximum instantaneous growth rate (at the tips of the continuous diameter of the unit circle) and the trajectory with initial condition of the eigenvector that produces maximum growth (at the tips of the dashed diameter of the unit circle). Both initial conditions result in large transient growth before their ultimate decay at the rate of the spectral abscissa (−1). As expected, the global optimal initial condition produces considerably more growth than does the vector associated with the numerical abscissa.

examine the optimal growth as a function of time t. This optimal growth is given by the spectral norm $\|e^{\mathbf{A}t}\|$, which is the maximum singular value of $e^{\mathbf{A}t}$. The global optimal is defined as the initial perturbation of unit norm that achieves maximum growth over all optimizing times. The phase plane trajectory of the global optimal is shown in Fig. 3 for $\theta = \pi/100$. The global optimal for this case turns out to be very close to the biorthogonal of the least damped eigenvector. This biorthogonal is easily seen to lie along the direction $(\sin\theta, -\cos\theta)$. We have seen in the previous section that the biorthogonal is the optimal excitation of the least-damped mode and that a $\csc\theta$ amplitude magnification of the least-damped mode arises from initially introducing the biorthogonal rather than the mode itself. It is instructive to confirm this argument though a direct calculation in this simple example.

The expression for the propagator at t is given by

$$e^{\mathbf{A}t} = \begin{pmatrix} e^{-t} & \cot\theta(e^{-2t} - e^{-t}) \\ 0 & e^{-2t} \end{pmatrix}, \qquad (37)$$

which in the limit $t \to \infty$ becomes

$$\lim_{t\to\infty} e^{\mathbf{A}t} \approx \begin{pmatrix} e^{-t} & -\cot\theta e^{-t} \\ 0 & 0 \end{pmatrix}, \qquad (38)$$

from which

$$e^{\mathbf{A}t}\begin{pmatrix} \sin\theta \\ -\cos\theta \end{pmatrix} = \csc\theta e^{-t}\begin{pmatrix} 1 \\ 0 \end{pmatrix}, \qquad (39)$$

verifying the optimal excitation of the mode by its biorthogonal and the $\csc\theta$ magnitude of the magnification.

The growth produced by the global optimal is plotted as a function of time in Fig. 4 for representative values of θ. A bound on nonnormal growth can be obtained in terms of the spectral condition number of the eigenvector matrix of the operator $\kappa(\mathbf{E}) \equiv \|\mathbf{E}\|\,\|\mathbf{E}^{-1}\|$ by considering the similarity transformation by the matrix of column eigenvectors of $\mathbf{A}$ as in (19):

$$\|e^{\mathbf{A}t}\| \leq \kappa(\mathbf{E})\|e^{\Lambda t}\| = \cot(\theta/2)e^{\lambda_{\max}t}. \qquad (40)$$

It can be seen from Fig. 4 that the bound (40) is not attained for this operator.

The frequency response for $\theta = \pi/10$ and $\pi/100$ is shown in Fig. 5. Also shown is the frequency response expected from traditional resonance arguments in which the response is obtained by summation of the contributions from the poles of the resolvent (16) as would be the case if the eigenvectors were orthogonal (which we have seen in this example occurs for $\theta = \pi/2$). As expected from the large nonnormal growth in this system, this equivalent normal response which neglects nonnormal amplification is orders of magnitude smaller than the actual response of the system and the variance calculated as the area under the nonnormal response curves greatly exceeds the equivalent normal

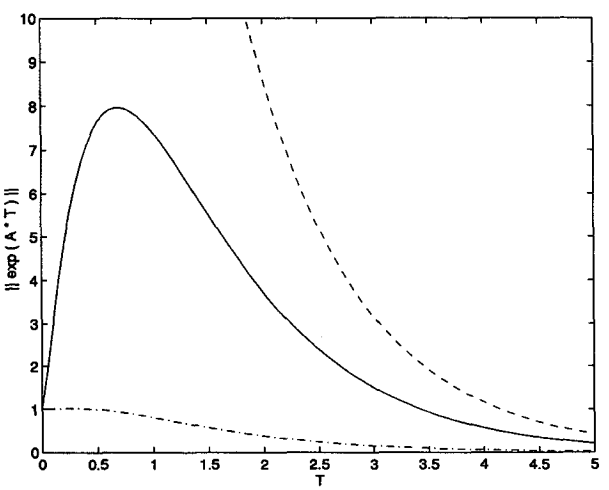

FIG. 4. The optimal growth in the simple 2 × 2 nonnormal matrix example with $\theta = \pi/100$ (solid line) and $\theta = \pi/10$ (dash-dot line) as a function of the interval of time over which the growth takes place. In addition, for the case of $\theta = \pi/100$, the bound provided by (40) is plotted as the upper dashed line.

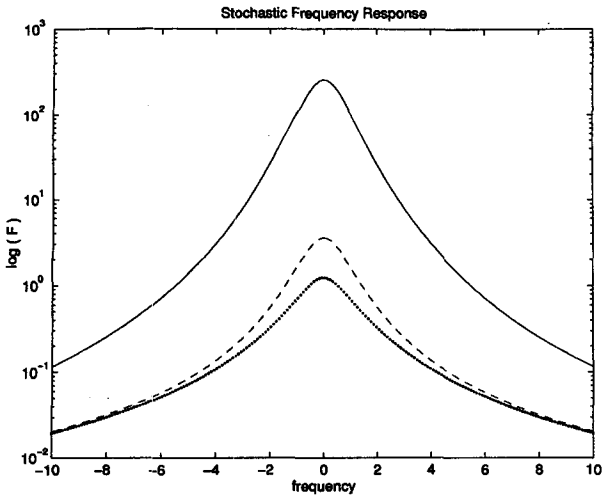

FIG. 5. The frequency response of the simple 2 × 2 nonnormal example showing the response to white noise forcing of unit amplitude with $\theta = \pi/100$ (upper solid line) and with $\theta = \pi/10$. The response of a normal matrix with the same spectrum corresponding to $\theta = 0$ is also shown (lower dot curve).

variance obtained as the area under the equivalent normal curve as is consistent with inequality (22).

Asymptotic stability ensures existence of stationary statistics, and the stochastic dynamic operator $\mathbf{B}^\infty$ for this system is easily computed:

$$\mathbf{B}^\infty = \int_0^\infty e^{\mathbf{A}^\dagger t} e^{\mathbf{A}t}\, dt = \frac{1}{2}\begin{pmatrix} 1 & -\dfrac{\cot\theta}{3} \\ -\dfrac{\cot\theta}{3} & \dfrac{1}{2}+\dfrac{\cot^2\theta}{6} \end{pmatrix}. \quad (41)$$

With unitary forcing ($\mathbf{F}\mathbf{F}^\dagger = \mathbf{I}$), the correlation matrix is

$$\mathbf{C}^\infty = \int_0^\infty e^{\mathbf{A}t} e^{\mathbf{A}^\dagger t}\, dt = \frac{1}{2}\begin{pmatrix} 1+\dfrac{\cot^2\theta}{6} & -\dfrac{\cot\theta}{6} \\ -\dfrac{\cot\theta}{6} & \dfrac{1}{2} \end{pmatrix}. \quad (42)$$

The operators $\mathbf{B}^\infty$ and $\mathbf{C}^\infty$ clearly differ except for the case when $\mathbf{A}$ is normal (i.e., $\theta = \pi/2$). The maintained variance given by the trace of either (41) or (42) is

$$\langle \|\mathbf{u}\|^2 \rangle = \frac{3}{4} + \frac{\cot^2\theta}{12}, \quad (43)$$

in which the 3/4 can be identified as the equivalent normal response. Equation (43) illustrates the fact that the variance maintained by nonnormal systems is necessarily greater than the equivalent normal variance based on traditional resonance arguments.

The stochastic optimal is the leading eigenvector of $\mathbf{B}^\infty$ and the first EOF is the leading eigenvector of $\mathbf{C}^\infty$. Only for normal $\mathbf{A}$ do these coincide with the least damped mode of the system. As nonnormality increases for $\theta \to 0$, the stochastic optimal, the leading EOF, the least-damped mode, and the eigenvector associated with the numerical abscissa obtain limiting orientations. These are shown in Figs. 6a and 5b, in which these unit vectors are plotted for $\theta = \pi/10$ and $\theta = \pi/100$. Note that as nonnormality increases, the stochastic optimal approaches the biorthogonal and the leading EOF approaches the mode itself because of the large nonnormal growth of the biorthogonal, in contrast to what obtains at moderate values of nonnormality ($\theta = \pi/10$) for which although there is no transient growth the nonnormality still forces all the vectors to be distinct.

b. A baroclinically unstable system

Traditional instability theory for synoptic- and planetary-scale dynamics is based on the work of Charney (1947) and Eady (1949), according to which the existence of an eigenvalue of the linearized baroclinic operator with positive real part determines the stability of perturbations. Because the baroclinic operator is nonnormal, eigenanalysis of the operator directly addresses only the $t \to \infty$ asymptotic. To obtain a description of baroclinic waves for all times, it is necessary to apply generalized stability analysis to the operator.

Consider for example the Eady model of baroclinic instability in which the background velocity profile varies linearly with height, stratification in the troposphere is assumed constant, variation of the Coriolis parameter is ignored, the Boussinesq approximation is made, and the sharp increase of stratification at tropopause level is modeled by imposition of a solid upper boundary. Conservation of perturbation potential vorticity defines a dynamical system (Gill 1982) of the general form (1):

$$\frac{\partial \phi}{\partial t} = (\nabla^2)^{-1}[-ikz\nabla^2\phi - r(x)\nabla^2\phi], \quad (44)$$

with boundary conditions expressing the conservation of potential temperature along the solid surfaces at the ground and tropopause:

$$\frac{\partial^2\phi}{\partial t\,\partial z} = -ikz\frac{\partial\phi}{\partial z} + ik\phi - r(x)\frac{\partial\phi}{\partial z} \quad \text{at} \quad z = 0, 1. \quad (45)$$

The perturbation geostrophic streamfunction has been assumed here to be of harmonic form in the zonal (x) and meridional (y) direction, $\phi(z, t)e^{ikx+ily}$. Time has been nondimensionalized by N/fS, with N the Brunt–Väisälä frequency frequency, f the Coriolis parameter, and S the shear. Vertical distance has been nondimensionalized by the height of the tropopause, H, and horizontal distances by NH/f.

The nondimensional potential vorticity operator is of the form $\nabla^2 = \partial^2/\partial z^2 - k^2 - l^2$ and imposition of the boundary conditions (45) renders this operator invert-

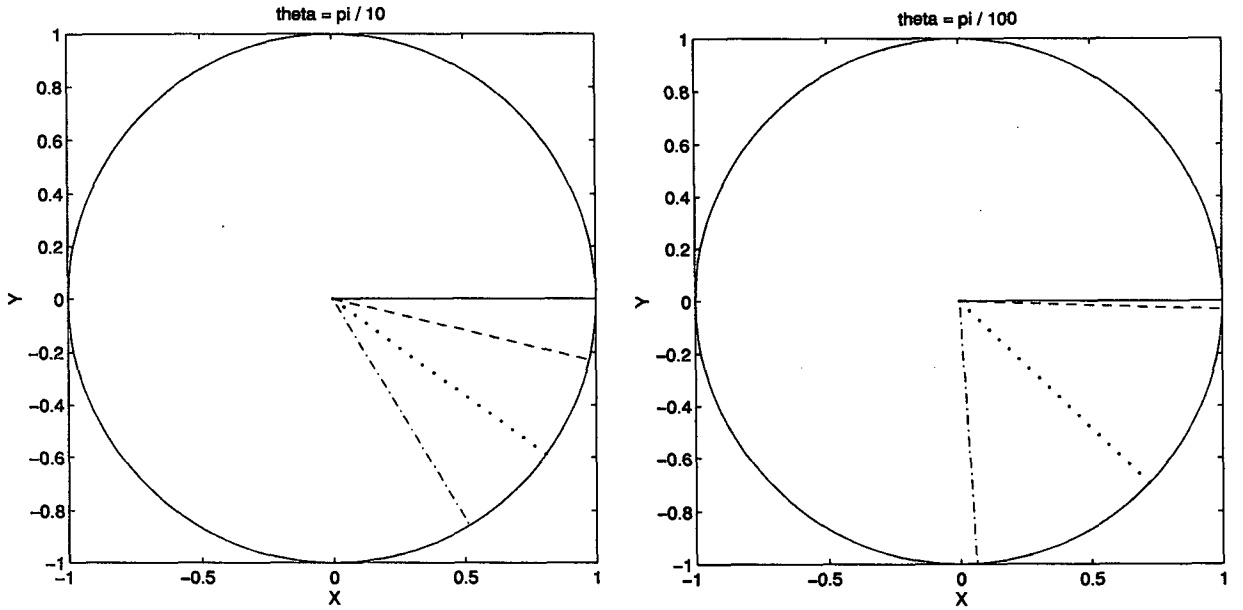

FIG. 6. Phase plane portrait of the least damped eigenvector (solid line), the first EOF (dash line), the numerical abscissa (dot line), and the stochastic optimal (dash-dot line) for the simple 2 × 2 nonnormal matrix example. The case of $\theta = \pi/10$ is shown in (a), the case of $\theta = \pi/100$ in (b). For a normal matrix all these eigenvectors would be identical.

ible. Zonally varying potential vorticity and thermal damping with coefficient $r(x)$ is allowed for but these dampings are taken zonally constant for this example.

The energy norm is defined as $(\phi^\dagger M\phi)^{1/2}$, where for a vertical discretization of grid size δz the metric is given by

$$M = \frac{\delta z}{4}\left[-\frac{d^2}{dz^2} + (k^2 + l^2)\mathbf{I}\right], \qquad (46)$$

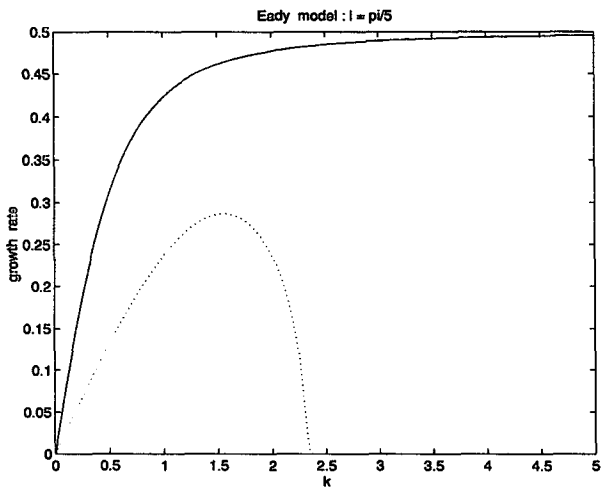

FIG. 7. The real part of the eigenspectrum of the undamped Eady model with meridional wavenumber $l = \pi/5$ is plotted as a function of zonal wavenumber (dotted line). In addition, the numerical abscissa is plotted as a solid line. Both the modal and nonmodal growth rates vanish in the limit $k \to 0$, but there is no counterpart to the modal shortwave cutoff in the numerical abscissa.

with $\mathbf{I}$ the identity. In order to assess the growth of perturbations in the energy norm, we define a generalized velocity $u = M^{1/2}\phi$ and proceed with the generalized stability analysis as described earlier.

The numerical abscissa (the instantaneous growth rate) and the spectral abscissa (the asymptotic growth rate) for the case $r(x) = 0$ are plotted in Fig. 7 as a function of the horizontal wavenumber k for $l = \pi/5$ (the results are generic and do not depend sensitively on the choice of the parameters).

Consider a zonal scale $k = 2.5$, which is on the stable side of the modal instability shortwave cutoff for the undamped Eady model that occurs at $k = 2.39$. Assume further a coefficient of thermal and potential vorticity damping of $r = 0.1$, which corresponds with a 40 m s^{-1} jet and a Rossby radius of deformation $NH/f = 1000$ km to an e-folding time of 2.9 days. Perturbations will asymptotically decay at the rate of the dissipation, but for intermediate times, calculation of the optimal energy growth as a function of optimizing time t demonstrates the existence of robust energy growth with a global optimal increase in energy by a factor of about 100 for an optimizing time of 4 days (Fig. 8). The two asymptotic growth rates in energy, the $t \to 0$ asymptotic growth rate given by twice the numerical abscissa and the $t \to \infty$ asymptotic growth rate given by twice the spectral abscissa, are also shown in Fig. 8.

Modal instability typically occurs over a restricted range of wavenumbers. This band of instability is bounded by a longest unstable wave (which may be infinite) and by a shortest unstable wave. The numerical abscissa, the global optimal, and the spectral ab-

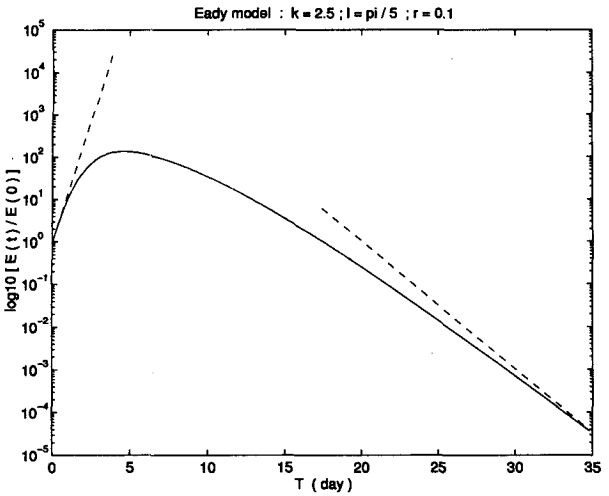

FIG. 8. The generalized stability portrait of the damped ($r = 0.1$) Eady model with meridional wavenumber $l = \pi/5$ and zonal wavenumber $k = 2.5$. The dashed line on the left indicates the initial energy growth rate and has slope twice the numerical abscissa. The dashed line on the right indicates the asymptotic energy decay rate and has slope twice the spectral abscissa. The solid line in between these asymptotes indicates the energy growth possible for an optimally configured initial perturbation; this growth is the square of the spectral norm of the Eady propagator at the indicated time.

scissa all vanish as $k \to 0$, so we may conclude that baroclinic conversion vanishes in this model for sufficiently long waves. On the other hand, as can be seen from Fig. 7, baroclinic conversions in the absence of strong dissipation continue for wavenumbers considerably in excess of the shortwave cutoff of modal instability (Farrell 1984, 1985; Joly 1995). Moreover, examination of Fig. 7 shows clearly that arguments based on energetics (such as extensions of the parcel argument for the existence of a wedge of instability), implying the necessity of a shortwave cutoff and a peak in growth rate at the modal instability maximum, cannot be valid.

We continue to consider zonal and meridional wavenumbers $k = 2.5$, $l = \pi/5$, respectively, and a coefficient of thermal and potential vorticity damping of $r = 0.1$, which corresponds to an e-folding time of 2.9 days and renders the dynamical operator in (44) asymptotically stable. Despite this strong perturbation damping, stochastic excitation of the zonal flow results in substantial accumulation of perturbation energy. The distribution of the stochastically maintained energy as a function of phase speed ($c = \omega/k$): $\mathbf{F}(\omega) = \text{trace}[\mathbf{R}(\omega)\mathbf{R}^{\dagger}(\omega)]$ [cf. (21)] is shown in Fig. 9. The equivalent normal response, which is the response of the operator with the same eigenvalues but with orthogonal eigenvectors, is also shown in Fig. 9 by the dashed line. Note the great disparity between the two curves and the enhanced variance sustained by the nonnormality of the operator. The two peaks that are discernible in the nonnormal response, but are barely noticeable in the equivalent normal response, correspond to the phase speeds of the upper and lower stable modes of the neutral Eady problem. The energy accumulated in these stable modes has been extracted by nonnormal interaction with the mean flow.

We calculate the stochastic operator in (27) $\mathbf{B}^{\infty}$ and correlation matrix $\mathbf{C}^{\infty}$ by solving the Lyapunov equations in (31). The eigenfunctions of $\mathbf{B}^{\infty}$ ordered by the magnitude of their eigenvalues are the stochastic optimals in the order of their contribution to the mean energy of the statistically steady state. Similarly, the eigenvalues of $\mathbf{C}^{\infty}$ give the EOFs of the steady state. The geopotential height field of the first stochastic optimal which accounts for 32% of the maintained perturbation energy, and the first EOF, which accounts for 69% of the variance, are shown in Figs. 10a and 10b, respectively.

Climate theories based on baroclinic wave transport have traditionally associated heat flux with exponential instability. This example demonstrates that the damped modes of the stochastically forced Eady problem are capable of substantial heat flux. For the parameters given above, the total northward heat flux at 30° latitude can be calculated following Farrell and Ioannou (1994b). It is found that for each W m^{-2} of stochastic forcing a heat flux of $\approx$0.5 PW is induced; and that the vertical distribution of this heat flux has the realistic structure shown in Fig. 11.

c. *Example of convective instability*

Modal instability is commonly found in idealized model examples that fail to account for the dissipation

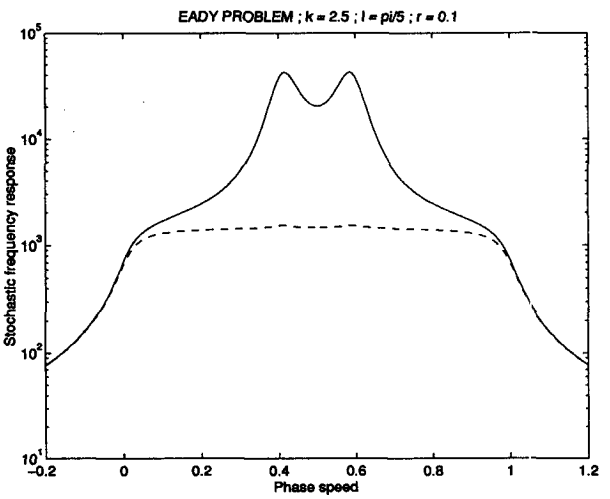

FIG. 9. The distribution of the stochastically maintained energy as a function of nondimensional phase speed in the Eady problem. The nondimensional zonal wavenumber is $k = 2.5$, the meridional wavenumber is $l = \pi/5$, and the thermal and potential vorticity damping coefficient is $r = 0.1$. Also shown (dashed line) is the response of a normal system with the same eigenspectrum. The peaks in the nonnormal response correspond to the phase speeds of the upper and lower stable modes of the neutral Eady problem.

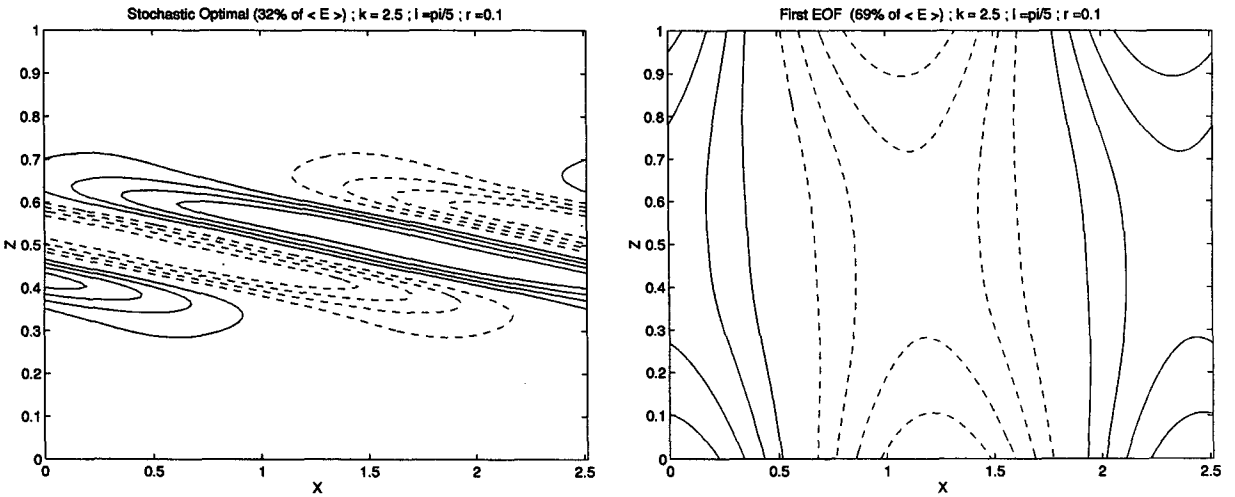

FIG. 10. The perturbation geopotential as a function of height (z) and zonal distance (x) for the stochastic optimal (a) and the first EOF (b) for the Eady problem with $k = 2.5$, $l = \pi/5$, and $r = 0.1$. When forced white in time the stochastic optimal pattern maintains 32% of the mean perturbation energy. The first EOF is the geopotential height pattern accounting for 69% of the mean perturbation energy.

and zonal confinement of the region of substantial baroclinicity in the midlatitude atmosphere. When proper account is taken of the limited extent of the baroclinic region (but not of realistic dissipation), only instabilities that we will refer to as convective are retained (Lin and Pierrehumbert 1993). Global stability analysis of such a problem will reveal no unstable modes and a comprehensive method of analyzing perturbation growth in the absence of local or global instability must be based on the underlying nonnormality of the necessarily asymptotically stable operator. However, traditional normal-mode-based analysis of convective instability relies on the assumption of asymptotic dominance of the approximate eigenmode of the associated zonally homogeneous problem (Merkine 1977; Simmons and Hoskins 1979; Farrell 1982b; Pierrehumbert 1984; DelSole and Farrell 1994). This approximation requires for its validity that the $t \to \infty$ asymptotic be obtained, a requirement unlikely to be satisfied in practice.

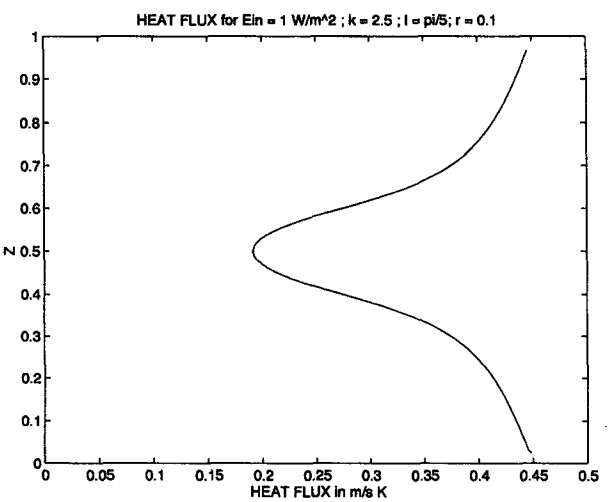

FIG. 11. The distribution of heat flux with height (m s^{-1} K) produced by waves with zonal and meridional wavenumber $k = 2.5$, $l = \pi/5$, respectively, when the Eady problem with damping coefficient $r = 0.1$ is stochastically forced with power of 1 W m^{-2}. The integrated heat flux over a latitude circle at 30° latitude is approximately 0.5 PW.

As an example of nonnormal analysis of a convective instability, consider the Eady model [Eqs. (44) and (45)] in a periodic channel of length X_m bounded by zonally localized regions of dissipation:

$$r(x) = \begin{cases} r\dfrac{1+\cos(\pi x/2)}{2} & \text{if } x \le 2 \\ r\dfrac{1+\cos[\pi(x-X_m)/2]}{2} & \\ & \text{if } x \ge X_m - 2. \end{cases} \tag{47}$$

We select $X_m = 20$ and $r = 100$ to ensure that no wave of significant amplitude tunnels through the region of dissipation. Under these circumstances, the eigenspectrum of the operator in (44) reveals only decaying modes. On the other hand there is robust perturbation growth that can be readily analyzed by determining the disturbance of optimal growth. For example, in Figs. 12a and 12b we plot the geostrophic streamfunction of the optimally growing perturbation over a period of 2 days at the initial and optimization time. The perturbation energy increases by a factor of nearly 112 over this time interval.

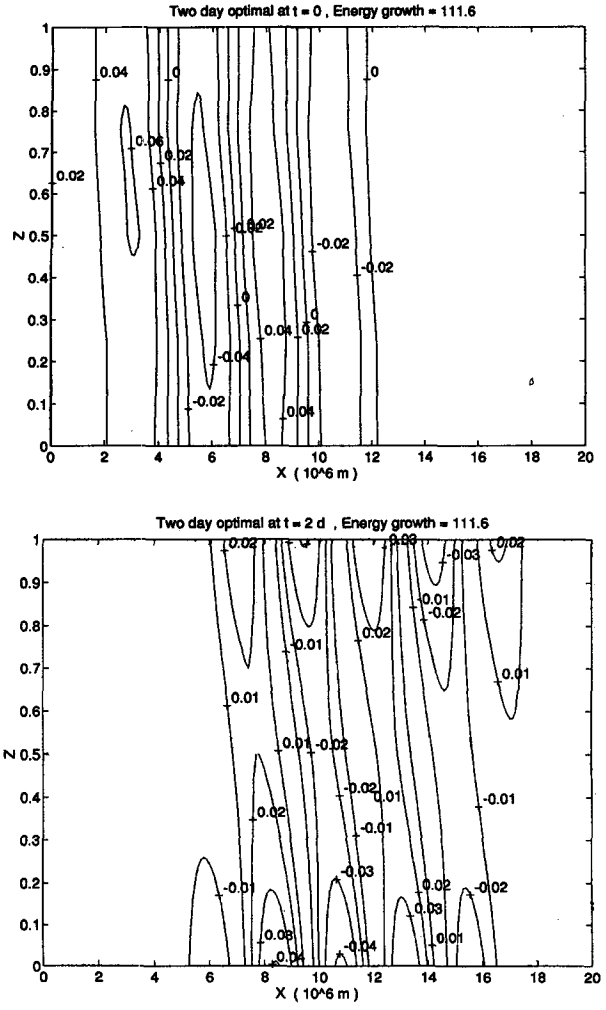

FIG. 12. The Eady model with meridional wavenumber $l = \pi/5$ and surface zonal velocity $U(0) = 0.15$. A localized region of high (10 day^{-1}) damping has been included within two nondimensional units corresponding to ($\pm$1000 km) on each end of the reentrant zonal boundary to prevent recirculation of waves. This model is absolutely stable, that is, an eigenanalysis shows no unstable modes. The potential for growth in this asymptotically stable system is expressed through the nonnormality of the Eady operator and this example shows (a) the two-day optimal initial perturbation and (b) this perturbation after two days, during which time perturbation energy has increased by a factor of 111.6.

5. Conclusions

Stability theory has traditionally been a foundation of physical understanding of dynamical systems in general and of atmospheric dynamics in particular. Traditionally stability theory has been based on the paradigm of Rayleigh (1880) and Kelvin (1887), in which the spectrum of the linearized dynamical system operator is analyzed for exponentially growing modes. In modal stability theory the possible nonorthogonality of the eigenvectors plays no role. It has been known since the time of Kelvin (1887) and Orr (1907) that this modal description is at best incomplete and that robust perturbation growth can occur without modal instabilities. Nevertheless, a full appreciation of the role of nonmodal growth in stability analysis is a recent development. In this work we have collected and organized recent advances into a systematic stability theory that comprises both the traditional $t \to \infty$ asymptotic results of modal theory and the transient growth phenomena at finite time that depend in an essential way on the nonnormality of the operator and the nonorthogonality of the eigenvectors.

The initial value problem for nonnormal operators is appropriate for analysis of cyclogenesis, episodic planetary wave amplifying events, and predictability on the forecast timescale. The timescale for such events is typically a small number of shear advection periods for the dominant wavenumbers that appropriately nondimensionalizes time for shear flow problems. The structural evolution of these synoptic- and planetary-scale disturbances during development is characteristic of the finite-time growth stage addressed by generalized stability theory.

In addition to phenomena such as cyclone formation and error growth that are appropriately addressed as initial value problems, there is another class of problems in which the nonnormality of the linearized operator is centrally involved, that being the dynamics of turbulence and particularly mechanisms maintaining the fully turbulent state. The model of turbulence based on nonnormal stochastic dynamics accounts directly for the transfer of energy from the background flow to the perturbations while parameterizing the role of nonlinearity both in forcing perturbations and in disrupting perturbation growth. This theory provides a physically based mechanistic picture of the turbulent state in which nonnormal growth rather than modal instability plays the central role. It is to be contrasted with the traditional theories of turbulence based on multiple instability transitions and the formation of internal unstable inflectional modes (Landau 1944).

The role of the parameterized nonlinear feedback in nonnormal turbulence theory has been illuminated by recent experiments with highly simplified nonnormal systems (Gebhardt and Grossman 1994; Baggett et al. 1995). Diagnosis from observations of the parameterization of nonlinearities in turbulence has recently been pursued using the fluctuation–dissipation relation (DelSole 1996).

In summary, reappraisal of linear theory in light of recent advances in understanding the deterministic and statistical dynamics of nonnormal systems has reinvigorated stability analysis and extended its scope of application; both as a calculational tool in areas such as predictability studies and as a mechanistic model in areas such as turbulence studies.

Acknowledgments. Discussions with Timothy DelSole are gratefully acknowledged. Brian Farrell was

supported in part by NSF ATM-9216813. Additional support was provided by the Department of Energy's (DOE) National Institute for Global Environmental Change (NIGEC) through the NIGEC Northeast Regional Center at Harvard University. (DOE Cooperative Agreement No. DE-FC03-90ER61010.) Financial support does not constitute an endorsement by DOE of the views expressed in this article.

REFERENCES

Baggett, J. S., T. A. Driscoll, and L. N. Trefethen, 1995: A mostly linear model of transition to turbulence. *Phys. Fluids A,* **7,** 833–838.

Blumenthal, M. B., 1991: Predictability of a coupled ocean–atmosphere model. *J. Climate,* **4,** 766–784.

Boberg, L., and U. Brosa, 1988: Onset of turbulence in a pipe. *Z. Naturforschung,* **43a,** 697–726.

Borges, M. D., and D. L. Hartmann, 1992: Barotropic instability and optimal perturbations of observed nonzonal flows. *J. Atmos. Sci.,* **49,** 335–354.

Branstator, G., 1985: Analysis of general circulation model sea surface temperature anomaly simulations using a linear model. Part II: Eigenanalysis. *J. Atmos. Sci.,* **42,** 2242–2254.

Breuer, K. S., and T. Kuraishi, 1994: Transient growth in two- and three-dimensional boundary layers. *Phys. Fluids A,* **6,** 1983–1993.

Buizza, R., and T. N. Palmer, 1995: The singular-vector structure of the atmospheric global circulation. *J. Atmos. Sci.,* **52,** 1434–1456.

Butler, K. M., and B. F. Farrell, 1992: Three dimensional optimal perturbations in viscous shear flow. *Phys. Fluids A,* **4,** 1637–1650.

Case, K. M., 1960: Stability of inviscid plane Couette flow. *Phys. Fluids,* **3,** 143–149.

Chang, J. J.-C., and M. Mak, 1995: Nonmodal barotropic dynamics of the intraseasonal disturbances. *J. Atmos. Sci.,* **52,** 896–914.

Charney, J. G., 1947: The dynamics of long waves in a baroclinic westerly current. *J. Meteor.,* **4,** 135–163.

Courant, R., and D. Hilbert, 1962: *Methods of Mathematical Physics.* Vol. II. Interscience Publishers, 830 pp.

DelSole, T. M., 1996: Can quasigeostrophic turbulence be modeled stochastically? *J. Atmos. Sci.,* **53,** 1617–1633.

——, and B. F. Farrell, 1994: Nonlinear equilibration of localized instabilities on a baroclinic jet. *J. Atmos. Sci.,* **51,** 2270–2284.

——, and ——, 1995: A stochastically excited linear system as a model for quasigeostrophic turbulence: Analytic results for one- and two-layer fluids. *J. Atmos. Sci.,* **52,** 2531–2547.

Drazin, P. G., and W. H. Reid, 1981: *Hydrodynamic Stability.* Cambridge University Press, 525 pp.

Eady, E. T., 1949: Long waves and cyclone waves. *Tellus,* **1,** 33–52.

Ehrendorfer, M., and R. M. Errico, 1995: Mesoscale predictability and the spectrum of optimal perturbations. *J. Atmos. Sci.,* **52,** 3475–3500.

Eliassen, A., 1956: Instability theories of cyclone formation. *Weather Analysis and Forecasting,* Vol. 1, S. Petterssen, Ed., McGraw-Hill, 305–319.

Farrell, B. F., 1982a: The initial growth of disturbances in a baroclinic flow. *J. Atmos. Sci.,* **39,** 1663–1686.

——, 1982b: Pulse asymptotics of the Charney baroclinic instability problem. *J. Atmos. Sci.,* **39,** 507–517.

——, 1984: Modal and nonmodal baroclinic waves. *J. Atmos. Sci.,* **41,** 668–673.

——, 1985: Transient growth of damped baroclinic waves. *J. Atmos. Sci.,* **42,** 2718–2727.

——, 1988a: Optimal excitation of neutral Rossby waves. *J. Atmos. Sci.,* **45,** 163–172.

——, 1988b: Optimal excitation of perturbations in viscous shear flow. *Phy. Fluids,* **31,** 2093–2102.

——, 1989a: Optimal excitation of baroclinic waves. *J. Atmos. Sci.,* **46,** 1193–1206.

——, 1989b: Transient development in confluent and diffluent flow. *J. Atmos. Sci.,* **46,** 3279–3288.

——, 1990: Small error dynamics and the predictability of atmospheric flows. *J. Atmos. Sci.,* **47,** 2409–2416.

——, and A. M. Moore, 1992: An adjoint method for obtaining the most rapidly growing perturbation to oceanic flows. *J. Phys. Oceanogr.,* **22,** 338–349.

——, and P. J. Ioannou, 1993a: Stochastic forcing of perturbation variance in unbounded shear and deformation flows. *J. Atmos. Sci.,* **50,** 200–211.

——, and ——, 1993b: Stochastic dynamics of baroclinic waves. *J. Atmos. Sci.,* **50,** 4044–4057.

——, and ——, 1993c: Stochastic forcing of the linearized Navier–Stokes equations. *Phys. Fluids A,* **5,** 2600–2609.

——, and ——, 1993d: Optimal excitation of three dimensional perturbations in viscous constant shear flow. *Phys. Fluids A,* **5,** 1390–1400.

——, and ——, 1993e: Perturbation growth in shear flow exhibits universality. *Phys. Fluids A,* **5,** 2298–2300.

——, and ——, 1993f: Transient development of perturbations in stratified shear flow. *J. Atmos. Sci.,* **50,** 2201–2214.

——, and ——, 1994a: Variance maintained by stochastic forcing of nonnormal dynamical systems associated with linearly stable shear flows. *Phys. Rev. Lett.,* **72,** 1188–1191.

——, and ——, 1994b: A theory for the statistical equilibrium energy spectrum and heat flux produced by transient baroclinic waves. *J. Atmos. Sci.,* **51,** 2685–2698.

——, and ——, 1995: Stochastic dynamics of the midlatitude atmospheric jet. *J. Atmos. Sci.,* **52,** 1642–1656.

——, and ——, 1996: Turbulence suppression by active control. *Phys. Fluids A,* **8,** 1257–1268.

Gebhardt, T., and S. Grossmann, 1994: Chaos transition despite linear stability. *Phys. Rev. E,* **50,** 3705–3711.

Gill, A. E., 1982: *Atmosphere–Ocean Dynamics.* Academic Press, 662 pp.

Golub, G. H., and C. E. Van Loan, 1989: *Matrix Computations.* The Johns Hopkins University Press, 642 pp.

Green, J., 1970: Transfer properties of large scale eddies and the general circulation of the atmosphere. *Quart. J. Roy. Meteor. Soc.,* **96,** 157–185.

Gustavsson, L. H., 1991: Energy growth of three-dimensional disturbances in plane Poiseuille flow. *J. Fluid Mech.,* **224,** 241–260.

Held, I. M., 1978: The vertical scale of an unstable baroclinic wave and its importance for eddy heat flux parameterizations. *J. Atmos. Sci.,* **35,** 572–576.

Henningson, D. S., and S. C. Reddy, 1994: On the role of linear mechanism in transition to turbulence. *Phys. Fluids A,* **6,** 1396–1398.

Ince, E. L., 1926: *Ordinary Differential Equations.* Dover, 558 pp.

Ioannou, P. J., 1995: Nonnormality increases variance. *J. Atmos. Sci.,* **52,** 1155–1158.

Joly, A., 1995: The stability of steady fronts and the adjoint method: Nonmodal frontal waves. *J. Atmos. Sci.,* **52,** 3082–3108.

Joseph, D. D., 1976: *Stability of Fluid Motions I.* Springer Verlag, 282 pp.

Kato, T., 1982: *A Short Introduction to Perturbation Theory of Linear Operators.* Springer Verlag, 161 pp.

Kelvin, Lord, 1887: Stability of fluid motions: Rectilinear motion of a viscous fluid between two parallel plates. *Phil. Mag.,* **24,** 188–196.

Kraichnan, R., 1976: Eddy viscosity in two and three dimensions. *J. Atmos. Sci.,* **33,** 1521–1536.

Lacarra, J.-F., and O. Talagrand, 1988: Short-range evolution of small perturbations in a barotropic model. *Tellus,* **40A,** 81–95.

Landau, L. D., 1944: Turbulence. *Dokl. Akad. Nauk SSSR,* **44,** 339–342.

Lin, C. C., 1961: Some mathematical problems in the theory of the stability of parallel flows. *J. Fluid Mech.,* **10,** 430–438.

Lin, S. J., and R. T. Pierrehumbert, 1993: Is the midlatitude zonal flow absolutely unstable? *J. Atmos. Sci.,* **50,** 505–517.

Lorenz, E. N., 1965: A study of the predictability of a 28-variable atmospheric model. *Tellus,* **17,** 321–333.

Merkine, L., 1977: Convective and absolute instability of baroclinic eddies. *Geophys. Astrophys. Fluid Dyn.,* **16,** 174–206.

Molteni, F., and T. N. Palmer, 1993: Predictability and finite time instability of the northern winter circulation. *Quart. J. Roy. Meteor. Soc.,* **119,** 269–298.

Montgomery, M. T., and B. F. Farrell, 1992: Polar low dynamics. *J. Atmos. Sci.,* **49,** 2484–2505.

Moore, A. M., and B. F. Farrell, 1993: Rapid perturbation growth on spatially and temporally varying oceanic flows determined using an adjoint method: Application to the Gulf Stream. *J. Phys. Oceanogr.,* **23,** 1682–1702.

Mureau, R., F. Molteni, and T. N. Palmer, 1993: Ensemble prediction using dynamically conditioned perturbations. *Quart. J. Roy. Meteor. Soc.,* **119,** 299–323.

Navarra, A., 1993: A new system of orthonormal modes for linearized meteorological application. *J. Atmos. Sci.,* **50,** 2569–2583.

Noble, B., and J. Daniel, 1988: *Applied Linear Algebra.* Prentice Hall, 521 pp.

Orr, W. Mc F., 1907: Stability or instability of the steady motions of a perfect liquid. *Proc. Roy. Irish Acad.,* **27,** 9–69.

Palmer, T. N., 1988: Medium and extended range predictability and stability of the Pacific/North American mode. *Quart. J. Roy. Meteor. Soc.,* **114,** 691–713.

Pedlosky, J., 1964: An initial-value problem in the theory of baroclinic instability. *Tellus,* **16,** 12–17.

Penland, C., and P. D. Sardeshmukh, 1995: The optimal growth of tropical sea surface anomalies. *J. Climate,* **8,** 1999–2024.

Petterssen, S., 1955: A general survey of factors influencing development at sea level. *J. Meteor.,* **12,** 36–42.

Pierrehumbert, R. T., 1984: Local and global instability of zonally varying flow. *J. Atmos. Sci.,* **41,** 2141–2162.

Rayleigh, J. W. S., 1880: On the stability, or instability, of certain fluid motions. *Proc. London Math. Soc.,* **9,** 57–70.

Reddy, S. C., 1993: Pseudospectra of Wiener-Hopf integral operators and constant-coefficient differential operators. *J. Integral Eq. Appl.,* **5,** 369–403.

——, and D. S. Henningson, 1993: Energy growth in viscous channel flows. *J. Fluid Mech.,* **252,** 209–238.

——, P. J. Schmid, and D. S. Henningson, 1993: Pseudospectra of the Orr–Sommerfeld operator. *SIAM J. Appl. Math.,* **53,** 15–47.

Roebber, P. J., 1984: Statistical analysis and updated climatology of explosive cyclones. *Mon. Wea. Rev.,* **112,** 1577–1589.

Schmid, P. J., and H. K. Kytomaa, 1994: Transient and asymptotic stability of granular shear flow. *J. Fluid Mech.,* **264,** 255–275.

Shepherd, T., 1985: On the time development of small disturbances to plane Couette flow. *J. Atmos. Sci.,* **42,** 1629–1642.

Simmons, A. J., and B. Hoskins, 1978: The life cycles of some nonlinear baroclinic waves. *J. Atmos. Sci.,* **25,** 414–432.

——, and ——, 1979: The downstream and upstream development of unstable baroclinic waves. *J. Atmos. Sci.,* **36,** 1239–1254.

Stone, P., 1978: Baroclinic adjustment. *J. Atmos. Sci.,* **35,** 561–571.

Trefethen, L. N., 1991: Pseudospectra of matrices. *Numerical Analysis,* D. F. Griffiths and G. A. Watson, Eds., Longman, 234–266.

——, A. E. Trefethen, S. C. Reddy, and T. A. Driscoll, 1993: Hydrodynamic stability without eigenvalues. *Science,* **261,** 578–584.

Vukicevic, T., 1993: Possibility of skill forecast based on the finite-time dominant linear solutions for a primitive equation regional forecast model. *J. Atmos. Sci.,* **50,** 1777–1791.

Zabczyk, J., 1975: A note on C_0-semigroups. *Bull. Acad. Polon. Sci.,* **23,** 895–898.